First-order quantum breakdown of superconductivity in an amorphous superconductor

Thibault Charpentier[1], David Perconte[1], Sébastien Léger[1], Kazi Rafsanjani Amin[1], Florent Blondelle[1], Frédéric Gay[1], Olivier Buisson[1], Lev Ioffe[2], Anton Khvalyuk[3], Igor Poboiko[4], Mikhail Feigel'man[3,5,6], Nicolas Roch[1] & Benjamin Sacépé[1] ✉

Continuous quantum phase transitions are widely assumed and frequently observed in various systems of quantum particles or spins. Their characteristic trait is a second-order, gradual suppression of the order parameter as the quantum critical point is approached. The localization of Cooper pairs in disordered superconductors and the resulting breakdown of superconductivity have long stood as a prototypical example. Here we show a departure from this paradigm, in which a discontinuous first-order quantum phase transition is tuned by disorder. We measure the plasmon spectrum in superconducting microwave resonators on amorphous superconducting films of indium oxide to provide evidence for a marked jump in both the zero-temperature superfluid stiffness and the transition temperature at the critical disorder. This discontinuous transition sheds light on the role of repulsive interactions between Cooper pairs and the subsequent competition between superconductivity and insulating Cooper-pair glass. Furthermore, we show that the critical temperature of the films no longer relates to the pairing amplitude but aligns with the superfluid stiffness, consistent with the pseudogap regime of preformed Cooper pairs. Our findings raise fundamental new questions about the role of disorder in quantum phase transitions and carry implications for superinductances in quantum circuits.

Superconductors undergo substantial changes in response to an increase in material disorder. Electron scattering, caused by disorder, increases resistivity and eventually leads to the breakdown of superconductivity due to Anderson localization and interactions[1]. This breakdown, commonly referred to as the superconductor–insulator transition (SIT), has long been considered a prototypical continuous quantum phase transition (QPT)[2,3], tunable by disorder, magnetic field or charge carrier density[1,2,4–6].

The hallmark of the transition and of its quantum critical point is the gradual suppression of the superconducting order parameter following scaling laws with critical exponents[2,4,6,7]. In disordered superconducting films, the central question has long been whether the amplitude (Cooper pairing)[8] or the phase (macroscopic coherence)[7] of the superconducting order parameter is suppressed at the critical disorder, offering two different paths with distinct outcomes[1].

In recent years, a body of work on thin films of various materials has revealed a more subtle interplay between phase and amplitude suppression[1]. Tunnelling spectroscopy experiments have provided evidence of pairing amplitude persisting across the transition[9–12], indicative of the localization of Cooper pairs in the insulator, together with strong

[1]Université Grenoble Alpes, CNRS, Grenoble INP, Institut Néel, Grenoble, France. [2]Google Research, Mountain View, CA, USA. [3]LPMMC, Université Grenoble Alpes, Grenoble, France. [4]Karlsruhe Institute of Technology, Karlsruhe, Germany. [5]CENN Nanocenter, Ljubljana, Slovenia. [6]Jožef Stefan Institute, Ljubljana, Slovenia. ✉e-mail: benjamin.sacepe@neel.cnrs.fr

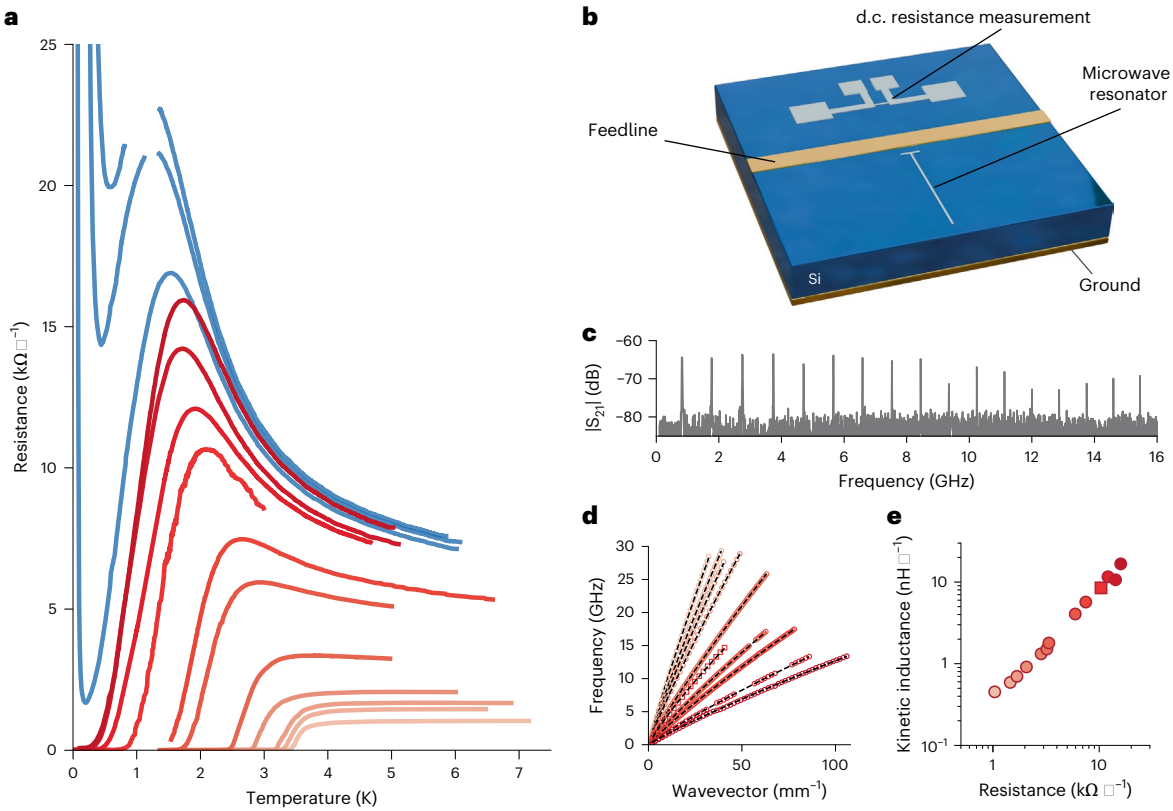

Fig. 1 | Resistivity and microwave spectroscopy of indium oxide striplines. **a**, Sheet resistance versus temperature for a series of a:InO thin films. As the sheet resistance increases, the critical temperature T_c of the superconducting films (red curves) decreases up to the transition to insulator (blue curves). **b**, Schematic of the sample featuring a microstrip microwave resonator coupled to a feedline and a four-terminal device for resistance measurements. **c**, Typical two-tone measurement trace providing the frequencies of resonant modes up to 30 GHz, here truncated to 16 GHz for clarity. **d**, Dispersion relations of plasma modes extracted from two-tone measurements for films of increasing disorder. The dashed lines are fits following the theoretical dispersion relation of plasmons (Methods). The only fitting parameter is the film's kinetic inductance. **e**, Kinetic inductance per square of the films extracted from dispersion relations, as a function of the maximum sheet resistance before the superconducting transition. On increase in disorder, the kinetic inductance grows by nearly two orders of magnitude. Interestingly, it exhibits a power-law dependence with sheet resistance with exponent 1.4. The symbol colours in **d** and **e** map to the line colours in **a**.

spatial fluctuations[9–11,13–15] and a pseudogap of preformed pairs[10,15–19]. Concomitantly, this was accompanied by a substantial suppression of the superfluid (phase) stiffness[15,18,20–22] on approaching critical disorder, pointing to a prevailing role of phase fluctuations[7,23]. Yet, scaling laws—the hallmark of continuous QPTs—have never been demonstrated for the superfluid stiffness[24] in disorder-tuned transitions.

Here we conducted a systematic study of the superfluid stiffness in one of the most disordered superconductors, amorphous indium oxide (a:InO) thin films, as we approach the breakdown of superconductivity by tuning disorder. Contrary to common expectations, we discovered that the superfluid stiffness does not exhibit a scaling behaviour with power-law suppression; instead, it shows a discontinuity at the critical disorder, signalling a first-order-type QPT. Furthermore, we show that at strong disorder, the superconducting transition temperature T_c is ruled by the superfluid stiffness in contrast to Bardeen–Cooper–Schrieffer (BCS) superconductors, corroborating the pseudogap of preformed pairs.

Superfluid stiffness

At the core of this study is the systematic and accurate measurement of the superfluid stiffness Θ together with the d.c. transport properties. The superfluid stiffness relates to the energy cost of twisting the superconducting phase φ, given by $E(\varphi) = \Theta \int d\mathbf{r} \frac{1}{2}|\nabla\varphi|^2$. A comparison of Θ with the other relevant energy scales of the superconducting state, such as the pairing gap and the superconducting transition temperature, provides a direct assessment of the role of phase fluctuations. A Θ value smaller than single-particle tunnelling gap Δ signals a phase-driven superconducting transition and the presence of preformed pairs[23,25]. It is worth noting that the effective dimensionality depends on the physical phenomenon under consideration: in our samples, it is three dimensional (3D) for Cooper pairing, two dimensional (2D) for phase fluctuations and one dimensional (1D) for plasmons. Methods provides further discussion on dimensionality.

We designed superconducting microwave stripline resonators (Fig. 1b) of a:InO, enabling us to directly extract the kinetic inductance per square of the materials, L_K, through the superconducting plasmon dispersion[26,27]. In the 2D limit, the superfluid stiffness straightforwardly follows from

$$\Theta = \left(\frac{\hbar}{2e}\right)^2 \frac{1}{L_K}, \quad (1)$$

where $\hbar$ is the reduced Planck constant and e is the electron charge.

Figure 1a displays the superconducting transition of the sheet resistance of a:InO thin films. On increasing disorder, characterized by the sheet resistance, the critical temperature continuously decreases (red curves), up to a critical value of resistance of $R^c_\square \simeq 16\ \text{k}\Omega$ above which more resistive films show a drop in resistance and a re-entrant insulating behaviour at the lowest T (blue curves). In the same cooldown of each sample, we systematically performed two-tone microwave spectroscopy of the resonators' surface plasmons, by taking advantage of the intrinsic nonlinearity of the superconductor (Methods).

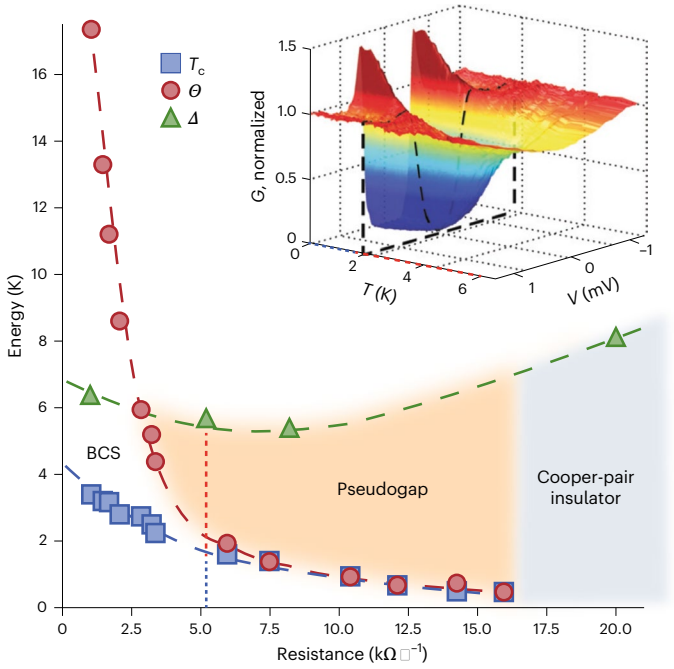

Fig. 2 | Phase-driven superconducting transition. Experimental phase diagram representing T_c, Δ (refs. 10,12,28) and the low-temperature Θ as a function of sheet resistance. The tunnelling data were obtained on virtually identical films[10,12,28], allowing a consistent comparison with the current microwave samples. On increase in disorder, that is, resistance, the superconductor goes from the BCS regime with $\Theta > \Delta$ and $T_c \propto \Delta$ to a phase-fluctuation regime characterized by $\Theta < \Delta$ and $T_c \approx \Theta$. In the latter, the superconducting transition is driven by the establishment of phase stiffness of preformed Cooper pairs that emerge as a pseudogap in the single-particle density of states. The blue, green and red dashed lines are guide for the eyes. The inset shows the normalized tunnelling conductance G measured on an a:InO film ($T_c = 1.7$ K) as a function of bias voltage across the tunnelling junction and temperature. The colours encode the values of the tunnelling conductance given in the vertical axis. The black dashed line marks the tunnelling spectrum at $T = T_c$. The pseudogap above T_c extends up to $\Delta \simeq 6$ K, in excellent agreement with the phase diagram. The dotted lines below (blue) and above (red) T_c in the inset are also reported in the figure at the corresponding disorder. Inset reproduced with permission from ref. 10, Springer Nature Limited.

The resulting plasmon modes (Fig. 1c) are straightforwardly indexed in frequency $2\pi f_n = v k_n$, where $k_n = n\pi/L$ is the wavevector for mode n and $v = 1/\sqrt{lc_k}$ is the velocity of the mode (L is the resonator's length and l and c_k are the inductance and capacitance per unit of length, respectively), leading to the plasmon dispersions shown in Fig. 1d.

The key to our analysis, the mode-dependent capacitance c_k to the ground plane in our straight stripline geometry, can be computed analytically (Methods). Consequently, the sublinear plasmon dispersions can be fitted with the inductance as a single adjustable parameter, yielding an accurate measurement of L_K. Consistent with expectations, we obtained a decrease in plasmon velocity, that is, the slope of the dispersion (Fig. 1d), with increasing disorder. This reflects the increase in L_K with sheet resistance (Fig. 1e), reaching a maximum value of 17 nH □$^{-1}$ at the transition to insulation. This value positions a:InO among the most inductive disordered superconductors, also known as superinductors[1], which exhibit wave impedance $Z = \sqrt{l/c_1}$ above the resistance quantum (Extended Data Fig. 3).

Strong phase fluctuations of preformed pairs

Translating the kinetic inductance into superfluid stiffness with equation (1) enables us to construct the complete phase diagram of the superconducting quantum breakdown of a:InO. In Fig. 2, we present the three energy scales characterizing the superconducting state: the critical temperatures T_c (Methods provides the definition), the single-particle tunnelling gaps Δ (refs. 10,12,28) and the superfluid stiffness Θ as a function of sheet resistance. Notice the non-monotonic evolution of the tunnelling gap that increases in the insulator as predicted by theory[29–32].

The dramatic effect of disorder on the superconducting order parameter is readily seen in the drop in Θ. At low disorder, for $R_\square < 3$ kΩ, the superfluid stiffness is larger than the pairing energy, $\Theta > \Delta$, indicating that the phase is stiff and the superconducting transition is governed by the pairing of electrons at T_c, according to BCS theory. However, for $R_\square > 3$ kΩ, the hierarchy of the two energy scales reverses: $\Theta < \Delta$. Strikingly, we also observe that $\Theta \simeq T_c$ over a wide range of disorder, from approximately 7 kΩ □$^{-1}$ (a value of the order of the resistance quantum for pairs $h/4e^2$) up to $R^c_\square$. In this range of disorder ($\Theta < \Delta$), the superconducting transition is entirely governed by phase fluctuations.

As earlier evidenced by tunnelling spectroscopy and discussed in other contexts[25,33,34], the scenario at play is that of the preformation of Cooper pairs at $T \approx \Delta$, followed at lower temperature by a wide regime of strong phase fluctuations also signalled by a pseudogap in the density of states[10] (Fig. 2, inset). Finally, at $T = T_c \simeq \Theta$, the phase of the order parameter becomes stiff, establishing the quasi-long-range order.

Such a redefinition of T_c is a direct consequence of the very low superfluid density, the 2D effective dimensionality (Methods provides dimensionality assessment) and the ensuing Berezinskii–Kosterlitz–Thouless (BKT) transition[35,36] observed in our data with a jump in superfluid density $\Theta(T_c^{BKT}) = \frac{2}{\pi} T_c^{BKT}$ (Extended Data Fig. 2). The relation $\Theta(T = 0) \simeq T_c$ naturally emerges in the 2D XY model and has been observed in some high-T_c-superconductor thin films[37–39]. More recently, similar studies in NbN films[11], granular aluminium[20], $LaAlO_3/SrTiO_3$ heterostructures[21] or amorphous MoGe[15] showed that Θ approaches T_c at strong disorder. Yet, a:InO stands out with an unprecedented large disorder range for $\Theta = T_c$ (Extended Data Fig. 1).

Superfluid stiffness discontinuity

This understanding of the superfluid stiffness provides definitive and compelling evidence for the scenario of preformed Cooper pairs in a:InO[10,19]. The question of their localization at the transition to insulator, which is central to this work, can now be addressed. Figure 3 shows the same data for Θ and T_c in semi-log scale. Although the continuous QPT paradigm would lead to a power-law suppression of Θ as one approaches the critical disorder, we instead observe a saturation of Θ at about 0.5 K, which abruptly drops at the onset of the insulator. This drop translates in a disappearance of the resonance once the sample is insulating. Likewise, given that $\Theta \simeq T_c$, the critical temperature exhibits a similar trend, also reaching approximately 0.5 K before vanishing.

A discontinuity in Θ as the pairing amplitude remains finite is a clear indication of the breakdown of the macroscopic phase coherence, implying a suppression of the superconducting order parameter. Therefore, the disorder-tuned transition to insulation in a:InO undergoes a first-order-type QPT. We conjecture that its origin lies in the overlooked Coulomb interaction between preformed (localized) Cooper pairs. By incorporating long-range interactions between pairs, the insulator is expected to form a Coulomb glass of pairs, which—according to earlier work[40,41]—possesses its own order parameter of the spin glass type. The corresponding ground-state energy of the glassy state (per the relevant volume) is given by the Coulomb energy E_C, which is proportional to the width of the Efros–Shklovsky Coulomb gap[42]. In this scenario, the SIT occurs between two ground states, each characterized by order parameters of distinct natures. The vanishing of the superconducting order parameter, coupled with the simultaneous appearance of the glassy order parameter, naturally manifests as an abrupt transition controlled by the competition between the free energies of these two very distinct phases of matter. In the $T = 0$ limit, the condition for the energy of the superconducting state to be equal

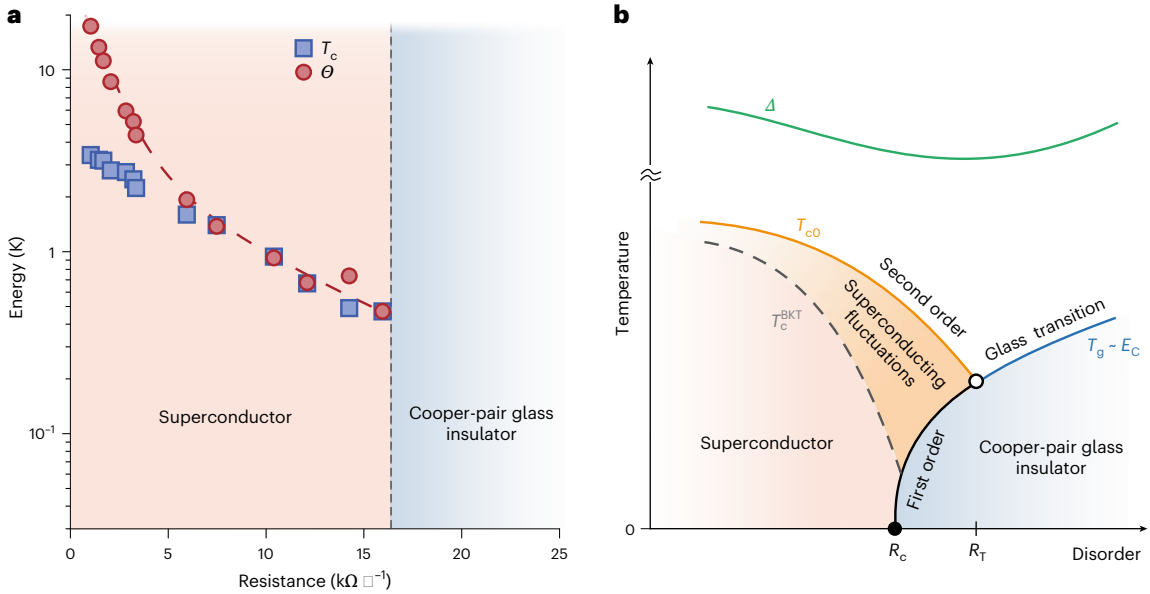

Fig. 3 | First-order quantum breakdown of superconductivity. a, Evolution of the low-temperature Θ and T_c with the sheet resistance in semi-log scale. At the critical disorder indicated by the vertical black dashed line, both Θ and T_c remain finite, saturating at about 0.5 K, without showing power-law suppression expected for quantum criticality in continuous QPTs. This abrupt, discontinuous suppression of superfluid density at the critical disorder indicates a first-order QPT. **b**, Phase diagram describing the competition between the superconducting phase and the Coulomb glass phase of localized Cooper pairs (Methods provides the theoretical justification). The superconducting transition is characterized by the mean-field critical temperature T_{c0} suppressed by disorder and interaction effects[8], and the BKT transition temperature T_c^{BKT} (refs. 35,36), marking the onset of quasi-long-range order. The single-particle gap Δ evolves non-monotonically across the transition, as observed experimentally (Fig. 2) and expected theoretically[29–32]. T_g is the glass transition temperature proportional to the Coulomb energy scale E_C (equation (2)), which evolves with disorder according to $E_C \approx 0.02\delta_{loc}$ (ref. 45), where δ_{loc} denotes the mean-level spacing in the localization volume. R_c marks the critical disorder separating the superconductor and Cooper-pair glass, whereas R_T is the resistance at the tricritical point, where the three transition lines meet. The re-entrant insulating behaviour emerges here due to the presence of a substantial region of temperature in which thermal superconducting fluctuations[48] can decrease the resistance and mimic a superconducting transition, only to be aborted by the onset of the Cooper-pair glass insulator.

to the energy of the insulating Coulomb glass state can be expressed by the relation[43]

$$\Delta_c \approx E_C = \sqrt{\pi \nu_0} \frac{e^3}{(4\pi\varepsilon_0\varepsilon)^{3/2}}, \quad (2)$$

where Δ_c is the superconducting collective gap right before the transition to insulator, which is substantially different from the single-particle spectral gap[19]. Here ν_0 is the density of states at the Fermi level and ε is the macroscopic dielectric constant in the insulating state. Note that equation (2) takes into account the fact that the elementary charge in our insulator is $2e$. It is important to highlight that the long-range Coulomb interaction driving the first-order transition is the interaction between bound electron pairs. The presence of a pseudogap in our strongly disordered films (Fig. 2 (inset) and refs. 10,19) provides experimental evidence for the existence of these pairs. Theoretically, ref. 43 explains why short-range electron repulsion[8] does not destroy the pairing itself. In short, this resilience is due to the fractal nature of electron wavefunctions in near-critical Anderson insulators.

The crucial consequence of equation (2) is the existence of a maximum value of the kinetic inductance L_K^{max} (or minimal value of superfluid stiffness Θ^{min}) achievable in a disordered thin-film superconductor. We can assess its order of magnitude by combining the semiclassical theory[44] relating L_K to the superconducting gap and the normal-state resistance, with the phase transition condition in equation (2), which leads to

$$\Theta^{min} \approx \frac{g}{8} E_C. \quad (3)$$

Here $g = h/(e^2 R_\square)$ is the dimensionless film conductance. With $\nu_0 = 2.4 \times 10^{46}\,J^{-1}m^{-3}$ (ref. 28) and $\varepsilon \approx 1{,}000$ for a:InO[45–47], as well as $g \approx 1.5$, we estimate Θ^{min} to be approximately 0.4 K, which closely aligns with the experimental value.

Phase diagram

The first-order nature of the transition is also reflected in the non-monotonic T dependence of resistance in insulating samples near the critical disorder (Fig. 1a). This re-entrant insulating behaviour can be understood in terms of the temperature-dependent competition between the free energies of the superconducting and Coulomb glass phases. As depicted in the phase diagram presented in Fig. 3b, which is based on experimental observations and theoretically substantiated in Methods, one can observe that just above the critical resistance R_c, as the temperature decreases below the superconducting mean-field transition temperature T_{c0}, a region characterized by strong superconducting fluctuations—including the classical BKT mechanism—emerges[48,49]. Initially, these fluctuations lead to a reduction in resistance. However, as the temperature continues to decrease, the transition to the Cooper-pair insulator glass occurs, thereby preventing the establishment of quasi-long-range order. The black solid line in Fig. 3b represents the first-order transition, originating from the quantum critical point (black dot) located at R_c, and extending to a tricritical point indicated by the open dot. Investigation into the physics surrounding the tricritical point would deserve further study.

A key implication of our work is that the properties of the disorder-tuned SIT depend on microscopic details of the material under consideration and, therefore, are not universal. For instance, for a first-order transition to occur, two conditions must be met: the superconductor must present a pseudogap (similar to NbN, TiN, granular Al and a few others), and the Coulomb gap amplitude must be comparable to the superfluid stiffness (as stated by equation (3)). These two conditions strongly depend on the parameters of the material such as dielectric constant and density of states. A first-order transition is anticipated in disordered materials exhibiting an anomalously long electric screening length l_{scr} comparable to the superconducting coherence length. In a:InO[41,43], the estimates for the dielectric constant ε in the insulating state[45,46] suggest $l_{scr} \approx \xi_{loc}$, where the localization length ξ_{loc} is approximately 4–5 nm, close to that of the superconducting coherence length[28]. Recent experiments in granular aluminium films also reported such a nanometre-scale screening length[50]. This material shares similar features with a:InO, such as a discontinuous drop in T_c at the SIT and non-monotonous re-entrant insulating state[51], suggesting a first-order breakdown of superconductivity here too. Interestingly, $LaAlO_3/SrTiO_3$ heterostructures[21] reach 80 nH $\square^{-1}$ at the transition, that is, $\Theta \approx 0.1$ K, which is consistent with a smaller Coulomb gap due to the large dielectric constant of $SrTiO_3$ known to be $\varepsilon \approx 10^4$.

Discussion

In a strongly disordered low-dimensional system, a first-order transition is not expected as disorder is known to smear the transition due to disorder-induced energy fluctuations and the pinning of domain walls that separate competing phases[52–54]. However, in a 3D system as ours, these effects do not necessarily preclude the existence of a sharp first-order transition in the thermodynamic sense. Yet, the observation of other distinct signatures of the first-order phase transition described above, such as glassy dynamics arising from the very slow motion of domain walls, would require the ability to continuously tune the parameters such as magnetic field[55] or carrier density via a gate voltage[21], which is beyond the scope of this study.

An important theoretical insight from our findings is the significant role of disorder in QPTs. Standard descriptions involve a mapping of QPTs in the D-dimensional system at $T = 0$ onto the classical thermal transition in dimension $D + 1$ (where 1 denotes the time dimension)[2,3]. Such correspondence is possible in clean systems because world lines in $D + 1$-dimensional space–time are not correlated in the time domain. By contrast, strong, 'frozen' disorder is, by definition, time independent, leading to world-line correlations in $D + 1$-dimensional space–time. This makes disorder markedly more influential in altering the nature of a QPT compared with a clean system and, thus, may call to revisit our understanding of disorder-tuned QPTs.

Finally, the emergence of materials with very large kinetic inductance, resulting from suppressed superfluid stiffness, underscores their potential significance for both quantum circuits and sub-terahertz photon detectors[1,56–58]. Superinductors capable of maintaining a quality factor greater than or of the order of 10^4 (Extended Data Fig. 4 and Methods provide details on the a:InO quality factor), combined with their compact footprint, offer versatility across various applications, ranging from inductively shunted qubits to dissipative resonators and nonlinear parametric amplification, as well as highly sensitive photon detectors. Our findings establish an upper limit for the highest achievable kinetic inductance in disordered materials. Nevertheless, the precise role of disorder in bulk dissipation remains a critical aspect yet to be fully understood[59], promising to stimulate further investigation and reveal new fundamental insights.

References

1. Sacépé, B., Feigel'man, M. & Klapwijk, T. M. Quantum breakdown of superconductivity in low-dimensional materials. *Nat. Phys.* **16**, 734–746 (2020).
2. Sondhi, S. L., Girvin, S. M., Carini, J. P. & Shahar, D. Continuous quantum phase transitions. *Rev. Mod. Phys.* **69**, 315–333 (1997).
3. Sachdev, S. *Quantum Phase Transitions* 2nd edn (Cambridge Univ. Press, 2011).
4. Goldman, A. M. & Markovic, N. Superconductor–insulator transitions in the two-dimensional limit. *Phys. Today* **51**, 39–44 (1998).
5. Gantmakher, V. F. & Dolgopolov, V. T. Superconductor–insulator quantum phase transition. *Phys.-Uspekhi* **53**, 1–49 (2010).
6. Lin, Y.-H., Nelson, J. & Goldman, A. Superconductivity of very thin films: the superconductor–insulator transition. *Phys. C* **514**, 130–141 (2015).
7. Fisher, M. P. A. Quantum phase transitions in disordered two-dimensional superconductors. *Phys. Rev. Lett.* **65**, 923–926 (1990).
8. Finkel'stein, A. Suppression of superconductivity in homogeneously disordered systems. *Phys. B* **197**, 636–648 (1994).
9. Sacépé, B. et al. Disorder-induced inhomogeneities of the superconducting state close to the superconductor–insulator transition. *Phys. Rev. Lett.* **101**, 157006 (2008).
10. Sacépé, B. et al. Localization of preformed Cooper pairs in disordered superconductors. *Nat. Phys.* **7**, 239–244 (2011).
11. Chand, M. et al. Phase diagram of the strongly disordered *s*-wave superconductor NbN close to the metal-insulator transition. *Phys. Rev. B* **85**, 014508 (2012).
12. Sherman, D. et al. Effect of Coulomb interactions on the disorder-driven superconductor-insulator transition. *Phys. Rev. B* **89**, 035149 (2014).
13. Kamlapure, A. et al. Emergence of nanoscale inhomogeneity in the superconducting state of a homogeneously disordered conventional superconductor. *Sci. Rep.* **3**, 2979 (2013).
14. Carbillet, C. et al. Spectroscopic evidence for strong correlations between local superconducting gap and local Altshuler-Aronov density of states suppression in ultrathin NbN films. *Phys. Rev. B* **102**, 024504 (2020).
15. Mandal, S. et al. Destruction of superconductivity through phase fluctuations in ultrathin a-MoGe films. *Phys. Rev. B* **102**, 060501 (2020).
16. Sacépé, B. et al. Pseudogap in a thin film of a conventional superconductor. *Nat. Commun.* **1**, 140 (2010).
17. Mondal, M. et al. Phase fluctuations in a strongly disordered *s*-wave NbN superconductor close to the metal-insulator transition. *Phys. Rev. Lett.* **106**, 047001 (2011).
18. Mondal, M. et al. Enhancement of the finite-frequency superfluid response in the pseudogap regime of strongly disordered superconducting films. *Sci. Rep.* **3**, 1357 (2013).
19. Dubouchet, T. et al. Collective energy gap of preformed Cooper pairs in disordered superconductors. *Nat. Phys.* **15**, 233–236 (2018).
20. Pracht, U. S. et al. Enhanced Cooper pairing versus suppressed phase coherence shaping the superconducting dome in coupled aluminum nanograins. *Phys. Rev. B* **93**, 100503 (2016).
21. Singh, G. et al. Competition between electron pairing and phase coherence in superconducting interfaces. *Nat. Commun.* **9**, 407 (2018).
22. Raychaudhuri, P. & Dutta, S. Phase fluctuations in conventional superconductors. *J. Phys. Condens. Matter* **34**, 083001 (2021).
23. Ghosal, A., Randeria, M. & Trivedi, N. Role of spatial amplitude fluctuations in highly disordered *s*-wave superconductors. *Phys. Rev. Lett.* **81**, 3940–3943 (1998).

24. Fisher, M. P. A., Weichman, P. B., Grinstein, G. & Fisher, D. S. Boson localization and the superfluid-insulator transition. *Phys. Rev. B* **40**, 546–570 (1989).
25. Emery, V. J. & Kivelson, S. A. Importance of phase fluctuations in superconductors with small superfluid density. *Nature* **374**, 434–437 (1995).
26. Mooij, J. E. & Schön, G. Propagating plasma mode in thin superconducting filaments. *Phys. Rev. Lett.* **55**, 114–117 (1985).
27. Camarota, B., Parage, F., Balestro, F., Delsing, P. & Buisson, O. Experimental evidence of one-dimensional plasma modes in superconducting thin wires. *Phys. Rev. Lett.* **86**, 480–483 (2001).
28. Sacépé, B. et al. High-field termination of a Cooper-pair insulator. *Phys. Rev. B* **91**, 220508 (2015).
29. Ma, M. & Lee, P. A. Localized superconductors. *Phys. Rev. B* **32**, 5658–5667 (1985).
30. Ghosal, A., Randeria, M. & Trivedi, N. Inhomogeneous pairing in highly disordered *s*-wave superconductors. *Phys. Rev. B* **65**, 014501 (2001).
31. Feigel'man, M., Ioffe, L., Kravtsov, V. & Cuevas, E. Fractal superconductivity near localization threshold. *Ann. Phys.* **325**, 1390–1478 (2010).
32. Bouadim, K., Loh, Y. L., Randeria, M. & Trivedi, N. Single and two-particle energy gaps across the disorder-driven superconductor–insulator transition. *Nat. Phys.* **7**, 884–889 (2011).
33. Eagles, D. M. Possible pairing without superconductivity at low carrier concentrations in bulk and thin-film superconducting semiconductors. *Phys. Rev.* **186**, 456–463 (1969).
34. Uemura, Y. J. et al. Universal correlations between T_c and $\frac{n_s}{m^*}$ (carrier density over effective mass) in high-T_c cuprate superconductors. *Phys. Rev. Lett.* **62**, 2317–2320 (1989).
35. Berezinskii, V. Destruction of long-range order in one-dimensional and two-dimensional systems possessing a continuous symmetry group. II. Quantum systems. *Sov. Phys. JETP* **34**, 610 (1972).
36. Kosterlitz, J. & Thouless, D. Ordering, metastability and phase transitions in two-dimensional systems. *J. Phys. C* **6**, 1181 (1973).
37. Lemberger, T. R., Hetel, I., Tsukada, A., Naito, M. & Randeria, M. Superconductor-to-metal quantum phase transition in overdoped $La_{2-x}Sr_xCuO_4$. *Phys. Rev. B* **83**, 140507 (2011).
38. Hetel, I., Lemberger, T. R. & Randeria, M. Quantum critical behaviour in the superfluid density of strongly underdoped ultrathin copper oxide films. *Nat. Phys.* **3**, 700–702 (2007).
39. Bozovic, I., He, X., Wu, J. & Bollinger, A. T. Dependence of the critical temperature in overdoped copper oxides on superfluid density. *Nature* **536**, 309–311 (2016).
40. Müller, M. & Ioffe, L. B. Glass transition and the Coulomb gap in electron glasses. *Phys. Rev. Lett.* **93**, 256403 (2004).
41. Müller, M. & Pankov, S. Mean-field theory for the three-dimensional Coulomb glass. *Phys. Rev. B* **75**, 144201 (2007).
42. Efros, A. L. & Shklovskii, B. I. Coulomb gap and low temperature conductivity of disordered systems. *J. Phys. C* **8**, L49 (1975).
43. Poboiko, I. & Feigel'man, M. Mean-field theory of first-order quantum superconductor-insulator transition. *SciPost Phys.* **17**, 066 (2024).
44. Mattis, D. C. & Bardeen, J. Theory of the anomalous skin effect in normal and superconducting metals. *Phys. Rev.* **111**, 412–417 (1958).
45. Feigel'man, M. V., Ivanov, D. A. & Cuevas, E. Dielectric response of Anderson and pseudogapped insulators. *New J. Phys.* **20**, 053045 (2018).
46. Ivanov, D. A. & Feigel'man, M. V. Low-energy dynamical response of an Anderson insulator with local attraction. *Phys. Rev. B* **95**, 045147 (2017).
47. Ebensperger, N. G. *Dielectric Properties on the Insulating Side of the Superconductor-Insulator Transition*. PhD thesis, Univ. Stuttgart (2021).
48. Larkin, A. & Varlamov, A. *Theory of Fluctuations in Superconductors* (Oxford Univ. Press, 2005).
49. Poboiko, I. & Feigel'man, M. Paraconductivity of pseudogapped superconductors. *Phys. Rev. B* **97**, 014506 (2018).
50. Kristen, M. et al. Giant two-level systems in a granular superconductor. *Phys. Rev. Lett.* **132**, 217002 (2024).
51. Levy-Bertrand, F. et al. Electrodynamics of granular aluminum from superconductor to insulator: observation of collective superconducting modes. *Phys. Rev. B* **99**, 094506 (2019).
52. Imry, Y. & Wortis, M. Influence of quenched impurities on first-order phase transitions. *Phys. Rev. B* **19**, 3580–3585 (1979).
53. Imry, Y. & Ma, S.-k Random-field instability of the ordered state of continuous symmetry. *Phys. Rev. Lett.* **35**, 1399–1401 (1975).
54. Vojta, T. Phases and phase transitions in disordered quantum systems. *AIP Conf. Proc.* **1550**, 188–247 (2013).
55. Crane, R. et al. Survival of superconducting correlations across the two-dimensional superconductor-insulator transition: a finite-frequency study. *Phys. Rev. B* **75**, 184530 (2007).
56. Grünhaupt, L. et al. Granular aluminium as a superconducting material for high-impedance quantum circuits. *Nat. Mater.* **18**, 816–819 (2019).
57. Hazard, T. M. et al. Nanowire superinductance fluxonium qubit. *Phys. Rev. Lett.* **122**, 010504 (2019).
58. Astafiev, O. V. et al. Coherent quantum phase slip. *Nature* **484**, 355–358 (2012).
59. Grünhaupt, L. et al. Loss mechanisms and quasiparticle dynamics in superconducting microwave resonators made of thin-film granular aluminum. *Phys. Rev. Lett.* **121**, 117001 (2018).

Methods

Samples

Our samples are disordered thin films of a:InO. Films with thickness of 40 nm are prepared by electron-beam evaporation of high-purity (99.999%) In_2O_3 onto a high-resistivity silicon substrate and maintaining a controlled O_2 partial pressure, enabling the tuning of disorder. Structures were patterned by electron-beam lithography on a polymethyl methacrylate resist, followed by development in isopropyl alcohol:water at a temperature of 4 °C. The back of the sample is coated with a thick layer of gold to act as a ground plane for the microstrip resonator. The latter comprises millimetre-long, 1-μm-wide lines (Extended Data Table 1 shows the exact sample geometries) and is accompanied with a co-evaporated Hall-bar structure of the same width (length, 10 μm), allowing the transport characterization of the films.

Measurement setup

The samples were placed in a copper sample holder shielded by mu-metal and connected to the input and output microwave lines. The d.c. lines are used for resistance measurements. The a:InO resistance of the transport mesa structure (Fig. 1b) was measured using the standard lock-in amplifier technique and an a.c. current bias of 0.1–1 nA. Microwave measurements were carried out in transmission with a vector network analyser and a second microwave source for the two-tone measurements.

The technique uses a microwave resonator with a simple straight stripline geometry, which can be probed at very low temperatures (20 mK), very low excitation powers (down to a few photons in average) and gigahertz frequencies (quantum regime $\hbar\omega \gg k_B T$). The cryostat in which the measurements took place is routinely used for the characterization of high-coherence superconducting circuits, providing a suitable filtered microwave environment. The originality of our experimental technique is the exploitation of the intrinsic nonlinearities of the superconductor (Kerr effect) using two-tone measurements for the detection of resonance modes over a large frequency range, far beyond the frequency bandwidth allowed by standard microwave components.

Two-tone spectroscopy

To experimentally obtain the dispersion relation of plasmons (Fig. 1d), we perform a two-tone measurement, a technique that exploits the intrinsic nonlinearity of current–phase relation in disordered superconductors. For a narrow superconducting wire of width w and length L at frequencies well below the gap ($\omega \ll \Delta$), the latter can be described by the following Hamiltonian (the derivation is provided elsewhere[60]):

$$H = \sum_n \hbar\omega'_n a_n^\dagger a_n - \frac{\hbar}{2}\sum_{n,m} K_{nm}\, a_n^\dagger a_n\, a_m^\dagger a_m, \tag{4}$$

where $a_n^\dagger$ and a_n are bosonic creation and annihilation operators for the normal 1D plasmonic modes of the stripline, $\omega'_n = \omega_n - (K_{nn} + \sum_m K_{nm})/4$ is the angular frequency of plasmonic mode n renormalized by the nonlinearity and K_{nm} is the Kerr coefficient.

A direct consequence of equation (4) is the decrease in the observed plasmonic frequency ω_n when other modes $m \neq n$ are populated: $\omega_n \to \omega'_n - \frac{1}{2}\sum_m K_{nm} N_m$, where $N_m = \langle a_m^\dagger a_m \rangle$ is the bosonic occupation number of mode m. The two-tone spectroscopy technique exploits this effect to accurately resolve the plasmonic spectrum. Using a vector network analyser, the minimum of the transmission amplitude at a given mode ω_n is continuously monitored, whereas an external microwave source generates a signal varied from 100 kHz to 20–30 GHz. When the source frequency is far from a resonant mode of the stripline, the frequency of the transmission minimum is not shifted. As the source frequency approaches ω_m, the frequency of mode n decreases due to the Kerr effect. This translates into a sudden increase in the transmission amplitude at ω_n and results in an easily identifiable peak (Fig. 1c).

For a moderately disordered superconductor described by a dirty-limit semiclassical theory, the Kerr coefficients can be calculated analytically, yielding[60]

$$K_{nm} = 3\gamma\left(1 - \frac{1}{4}\delta_{nm}\right)\frac{\xi^2}{Lw}\,\frac{\hbar\omega_n\omega_m}{\Theta}, \tag{5}$$

where ξ is the dirty-limit superconducting coherence length, Θ is the superfluid stiffness, $\gamma = \frac{\pi}{4} + \frac{3}{4\pi} \approx 1.02$ is determined by the current–phase nonlinearity of a diffusive superconductor and $\delta_{nm} = \begin{cases} 0 \text{ if } n \neq m \\ 1 \text{ if } n = m \end{cases}$.

In this estimation, we have assumed that the kinetic inductance fraction $\alpha = L_K/L_{tot} = 1$, that is, the geometric inductance of the wire is negligible compared with the kinetic inductance, as is the case for disordered indium oxide. For a strongly disordered superconductor, the semiclassical description is rendered inapplicable due to both strong localization and the presence of a pseudogap; hence, the exact value of K_{nm} is not known. However, one can still use equation (5) to estimate the order of magnitude of the effect.

Extracting L_K from the plasmon dispersion

Surface plasmons in a thin, long and narrow ($d \ll w \ll L$) superconducting wire follow the sound-like dispersion relation $\omega_k = |k|/\sqrt{lc_k}$, where l and c_k are the inductance and capacitance per unit length, respectively, and k is the wavevector. The restoring force responsible for charge-density oscillations is the Coulomb interaction between distant charges, whose long-range character induces a weak k dependence of the capacitance c_k (ref. 26). In our particular geometry (Fig. 1b), one also needs to account for screening effects of the silicon substrate (thickness $h = 300$ μm, with relative permittivity $\varepsilon = 11.9$) and the metallic ground plane underneath. This treatment is described elsewhere[60]. Here we show the resulting capacitance c_k for two limiting cases:

$$\frac{1}{c_k} = \begin{cases} \dfrac{1}{\pi\varepsilon_0(1+\varepsilon)}\ln\left[\dfrac{8h}{wk^{\delta(\varepsilon)}}\right] & \text{if } k \ll h^{-1}, \\ \dfrac{1}{\pi\varepsilon_0(1+\varepsilon)}\ln\left[\dfrac{8}{kwk^{\gamma}}\right] & \text{if } w^{-1} \gg k \gg h^{-1}, \end{cases} \tag{6}$$

where $\gamma \approx 0.577$ is the Euler–Mascheroni constant and

$$\delta(\varepsilon) = \frac{2\varepsilon}{1+\varepsilon}\sum_{j=1}^{\infty}\left(\frac{1-\varepsilon}{1+\varepsilon}\right)^{j-1}\ln\left[\frac{1}{j}\right]. \tag{7}$$

At low $k \ll h^{-1}$, the screening is efficient and the dispersion relation is linear, namely, $\omega(k) \propto k$, as first observed experimentally in another work[27]. At larger $k \gg h^{-1}$, the dispersion curve bends down via a logarithmic correction, which was predicted elsewhere[26]. Equation (6) describes the plasmonic spectrum for $k \ll w$, that is, in the region of 1D plasmons. The open-boundary conditions at each end of the stripline of length L implies the quantization of the wavevector for resonant mode n as $k_n = n\pi/L$ (where $n = 1, 2\ldots$).

The model above accurately accounts for the geometry of our samples, leaving the kinetic inductance per square $L_K = lw$ as the only fitting parameter. The reliability of the extraction of L_K has been confirmed by electromagnetic simulations in this geometry (Supplementary Section I) and therefore offers high accuracy in determining the superfluid stiffness. This accuracy is further demonstrated by the excellent agreement between microwave and d.c. measurements. Note that contrary to most other experimental probes of the superfluid response (two-coil mutual inductance, scanning superconducting quantum interference device, microwave spectrometer and so on), we do not need any calibration of the experimental setup or background subtraction to extract the kinetic inductance. We also note that the obtained L_K values are orders of magnitude larger than geometric inductances, thereby confirming the assumption of $\alpha = 1$.

Determination of critical temperature

In a disordered superconductor with low superfluid stiffness, three distinct critical temperatures can be defined: first, the critical temperature predicted by BCS theory, denoted as T_{c0}; second, a temperature $T_c < T_{c0}$ that incorporates the effects of various superconducting fluctuations; and finally, the BKT transition temperature $T_{BKT} < T_c$, below which superconductivity breaks down due to the unbinding of vortex pairs. These last two temperatures depart on the increase in disorder[48]:

$$\frac{T_{BKT} - T_c}{T_c} \approx -4\,\mathrm{Gi}\,, \tag{8}$$

where $\mathrm{Gi} = 7\zeta(3)e^2R_\square/(h\pi^3)$ is the Ginzburg–Levanyuk number and $R_\square$ is the normal-state sheet resistance measured above T_c. The mean-field temperature is also suppressed, as

$$T_c = T_{c0}\left(1 - 2\,\mathrm{Gi}|\ln \mathrm{Gi}\,|\right). \tag{9}$$

We determine our critical temperatures (T_c) by identifying the temperature at which a linear extrapolation of the $R(T)$ curves intersects the x axis (Fig. 1). Although this method does not yield the exact determination of T_{BKT}, which typically requires a multiparameter fit of the $R(T)$ curves (as demonstrated in ref. 61), we are confident that our extracted values fall in the range of $T_{BKT} \leq T_c^{exp} < T_c$. Moreover, the measurement of the temperature dependence of the superfluid stiffness (Extended Data Fig. 2) enabled us to accurately determine T_{BKT} for a highly disordered sample (DP-Res11). We concluded that our assessment of T_c deviates from T_{BKT} by less than 25%. Hence, our methodology for estimating T_c from transport measurements is sufficiently accurate for the discussions presented in the main text.

Effective dimensionality of a:InO films

The thickness of our films is $d = 40$ nm, which is approximately an order of magnitude larger than the low-temperature superconducting coherence length $\xi(0)$[28]. Consequently, the low-temperature behaviour of our system should be described as effectively 3D (bulk). Specifically, we applied the 3D theory of the $T = 0$ superconductor–Coulomb glass transition and derived the condition in equation (2). However, the transition out of the superconducting state driven by temperature differs in terms of dimensionality. Given the very low superfluid stiffness of a:InO films in the pseudogap regime, long-range phase fluctuations emerge as the primary driving force of the transition, leading to a mechanism akin to vortex–antivortex de-pairing[25], reminiscent of the 2D BKT transition[35,36]. Finally, our system is 1D with respect to plasmons—collective excitations with wavelengths much longer than the 1 μm width w of our superconducting stripes (Fig. 1d). This is the reason for these excitations to be ineffective in terms of thermodynamics: their density of states is too low at the microscopic scale. In addition, the effective magnetic penetration depth is also much longer than w.

To summarize, one should consider our system to be effectively 1D, 2D or 3D depending on the mechanism at play. Although long-wavelength plasmons responsible for microwave resonances and the Kerr effect are 1D, the effect of thermal phase fluctuations near T_c giving rise to the relation $T_c = \Theta$ is of a 2D nature, as expected from the BKT mechanism. Microscopic effects of disorder, local superconducting pairing and Coulomb repulsion occur on shorter scales than the film dimensions and are 3D in nature.

Phase diagram of a strongly disordered superconductor

The determination of the position of the first-order SIT at $T = 0$, given by equation (2), stems from a comparison between the ground-state energy densities of the superconducting and insulating states[43]. The free-energy density of the Coulomb glass state was calculated by solving the Parisi equations, and is expressed in terms of the key parameter E_C defined by the right equality in equation (2). This expression for E_C takes into account the charge $2e$ of a Cooper pair as well as the large dielectric constant ($\varepsilon \simeq 1{,}000$) of the underlying Anderson insulator of localized electrons[45–47]. Note that the energy E_C is proportional to (although differing by some numerical factor) the width of the Efros–Shklovsky Coulomb gap for this Cooper-pair insulator. For calculating the free energy of the superconducting state in ref. 43, we take into account the effect of the superconducting order parameter Δ on the Coulomb screening energy, which leads to an increase in energy as $\propto \nu_0|\Delta|E_C$. Such an effect is relevant in our problem even though it is totally negligible in usual metallic superconductors. This is because the electric screening length in an Anderson insulator is comparable to both localization length and superconducting coherence length. A key assumption in our calculation was to treat the order parameter Δ as a constant throughout the system. In fact, relatively close to the SIT, the order parameter starts to fluctuate rather strongly from one point to another[10]; for this reason, the left (approximate) equality in equation (2) may contain an unknown factor of the order of unity.

The phase diagram presented in Fig. 3b is the result of a delicate interplay between several phenomena: strong disorder of the superconducting phase, formation of the Coulomb glass in the insulating state, the physics of the resulting first-order phase transition and various manifestations of superconducting fluctuations in the insulating phase.

We start by discussing the phase diagram of a bulk superconductor (for example, a film of very large thickness), where the broadening of the superconducting transition due to fluctuations is essentially absent. At a low temperature, the phase transition happens between the superconductor and the Cooper-pair glass insulator, and therefore, this transition is of the first order.

The transition line between the full and empty black dots in Fig. 3b corresponds to the equality of the free energies of the two phases. The free energy of the Cooper-pair glass, denoted as $\delta F_C(T)$, behaves as $F_C(T) - F_C(0) \approx -E_C(T/E_C)^4$, reflecting the quadratic shape of the soft Coulomb gap, $\nu(E) \propto E^2$ (ref. 42). By contrast, the free energy of a strongly disordered superconductor, denoted as $\delta F_S(T)$, approximately scales as $-T_0(T/T_0)^{\beta+1}$, where the experimentally observed values are $T_0 \approx 10$ K and $\beta \approx 1.6$ (ref. 60). This power-law suppression with temperature of the superfluid stiffness Θ in our samples[60] arises from the strong inhomogeneity of the superconducting state, allowing 3D small-scale low-energy excitations to contribute to the free energy[60].

For disorder slightly above the critical value (Fig. 3b, black dot), the higher ground-state energy of the superconducting state can be compensated at a finite temperature by the higher entropy of this phase, resulting in $\delta F_S(T) < \delta F_C(T)$. Consequently, the first-order transition line initially trends towards higher temperatures with increasing disorder. In other words, the superconductor emerges as the high-temperature phase for this first-order phase transition. This contrasts with the classical BCS-like exponential dependence of the free energy, $\delta F_S(T) \propto -\exp(-\Delta/T)$, which would naturally lead to a conventional downward slope in the SIT line.

Note that the above arguments rely on the quadratic energy dependence of the soft Coulomb gap $\nu(E) \propto E^2$, implicitly assuming the irrelevance of certain local two-level systems (TLS) typically found in glasses, which have a nearly constant density of states. Although mean-field Coulomb glass theory[40] does not incorporate such TLS, corrections to the mean-field approximation could result in their apparition. However, in our problem, deviations from this mean-field approximation are expected to be very small, on the order of $\sim E_C/E_F \ll 1$. Therefore, the apparent absence of these TLSs seems natural.

At sufficiently high disorder, on the other hand, the Coulomb glass turns into a trivial Cooper-pair insulator via a glass transition[40,41], described by the transition line originating from the the tricritical point shown in Fig. 3b (empty dot). This inevitably implies the existence of yet another transition line (also starting from the empty dot on the phase diagram) separating the trivial insulator phase from the

superconducting one. Here the transition is of the second order, as observed experimentally[10] and predicted by the existing theory of SIT in the absence of Coulomb interaction[31]. This latter transition is described by the standard phenomenology, including the pronounced fluctuation effects in thin films.

In particular, as the film thickness decreases, the onset of superconductivity is pushed to lower temperatures (Fig. 3b, dashed line) by superconducting fluctuations and the BKT mechanism[48], accompanied with a gradual drop in resistance as one approaches the superconducting phase. Parallelly, the resistance of the Cooper-pair glass insulator in a certain range of temperatures is decreased by the existence of superconducting puddles, an inevitable consequence of the phase coexistence at the first-order phase transition. These two mechanisms underlie the intermediate drop in resistance of the insulating samples (Fig. 1a), before this trend is sharply reversed by the phase transition to the Coulomb glass.

Importantly, however, the span of the first-order transition line (Fig. 3b, between the full black and empty dots) is expected to be rather short. Indeed, the overall magnitude of the effect of the aforementioned low-energy excitations in strongly disordered superconductor is small[60], as evident by the fact that T_0 (featuring in the free-energy decrease δF_S) tends to be 5–10 times larger than the superconducting transition temperature T_{c0}, and, consequently, E_C via equation (2). The balance of the free energies then implies that the corresponding 'anomalous' direction of the transition line is only expected in a narrow temperature window. Specifically, the temperature corresponding to the tricritical point (Fig. 3b, empty dot) is estimated as $T_T \lesssim E_C(E_C/T_0)^{\beta/(3-\beta)} \ll E_C \approx T_{c0}$, with $\beta \approx 1.6$ and $T_0/E_C \approx 7$ already rendering $T_T \lesssim 0.1E_C$. Consequently, probing the vicinity of the transition point experimentally is challenging, as it is hard to continuously tune disorder.

Quantum phase slips rate estimation

A discontinuity of Θ as the pairing amplitude remains finite echoes of the superfluid jump at the quantum BKT transition in the $(1+1)$-DXY model. In this model, a superfluid jump is expected to occur at a critical wave impedance of $Z_c = \sqrt{l_c/c_1} = \frac{1}{3}\frac{h}{4e^2}$ (ref. 62), where l_c is the critical inductance (superfluid stiffness) at the jump. This jump marks the transition from a superfluid state to a Bose glass phase, characterized by the proliferation of quantum phase slips[63]. In our resonators, the surface plasmons are indeed 1D electromagnetic modes.

The quantum phase-slip rate in superconducting wires can be calculated knowing the superconducting gap Δ, wire dimensions and normal-state resistance per square $R_\square$ (ref. 64). In strongly disordered superconductors with a pseudogap of preformed pairs, such an expression cannot hold and one must instead turn to the framework described in ref. 31, leading to the estimate of the phase-slip amplitude[58]:

$$h\gamma_{QPS} \approx \Theta\sqrt{\frac{L}{w}}\exp\left(-\eta w\sqrt{\Theta\nu d}\right), \tag{10}$$

where $\eta \approx 1$ is a dimensionless constant, Θ is the 2D superfluid stiffness, d is the film thickness and ν is the single-particle density of states. Using $\nu = 2.4\times10^{46}\,\mathrm{J^{-1}\,m^{-3}}$ for indium oxide, $d = 40$ nm and width $w = 1\,\mu$m gives the estimation $h\gamma_{QPS} \approx 10^{-34}$ K for our most disordered sample (having $\Theta = 0.5$ K). The reason for such a low phase-slip rate is the large cross-section of our films. In comparison, a:InO nanowires in ref. 58 had width $w = 40$ nm and a phase-slip amplitude $h\gamma_{QPS} \approx 0.2$ K.

Consequently, the quantum phase-slip rate $h\gamma_{QPS}$ is completely negligible due to the large width (1 μm) of our resonators, thereby excluding this scenario. Furthermore, the wave impedance of all our resonators is well above Z_c (Extended Data Fig. 3), reaching up to $Z \approx 3\frac{h}{4e^2}$ at the critical disorder.

Dissipation in a:InO resonators

Dissipation in our resonators manifests through the value of the internal quality factor, which is extracted from fitting the microwave transmission spectrum (Supplementary Information and Supplementary Fig. 2).

Extended Data Fig. 4a,b displays the typical evolution of Q_i as a function of photon numbers and temperature, respectively. As a function of photon number, Q_i increases continuously. As a function of temperature, Q_i is non-monotonic: it initially decreases when warming up and then increases up to $T \approx 0.4$ K and decreases at higher T. Such dissipation behaviours are commonly accounted for by the presence of a bath of TLS that saturates on increasing the photon number or temperature[65], with the decrease at higher T being attributed to thermally activated quasiparticle dissipation[44]. Overall, for most a:InO resonators, we obtained $Q_i \approx 10^4$ at low photon number and low temperature.

Contrary to clean superconductors, dissipation in our a:InO resonators is not limited by surface TLSs. This is evidenced by the fact that resonators measured in a 3D cavity, for which the surface participation ratio is reduced by one order of magnitude, exhibit the same quality factor (Extended Data Fig. 4). Furthermore, to exclude the possibility of surface oxide contribution, we studied similar stripline resonators capped with a thin oxidized aluminium layer, which showed no change in Q_i (Extended Data Fig. 4a). This leads to the conclusion that dissipation in a:InO is predominantly bulk related and therefore associated with disorder, in accordance with other inductive materials[50,59,66].

Data availability

Source data are provided with this paper. All other data that support the plots within this paper and other findings of this study are available from the corresponding author upon reasonable request.

References

60. Khvalyuk, A. V., Charpentier, T., Roch, N., Sacépé, B. & Feigel'man, M. V. Near power-law temperature dependence of the superfluid stiffness in strongly disordered superconductors. *Phys. Rev. B* **109**, 144501 (2024).
61. Weitzel, A. et al. Sharpness of the Berezinskii-Kosterlitz-Thouless transition in disordered NbN films. *Phys. Rev. Lett.* **131**, 186002 (2023).
62. Giamarchi, T. & Schulz, H. J. Anderson localization and interactions in one-dimensional metals. *Phys. Rev. B* **37**, 325–340 (1988).
63. Kuzmin, R. et al. Quantum electrodynamics of a superconductor–insulator phase transition. *Nat. Phys.* **15**, 930–934 (2019).
64. Arutyunov, K., Golubev, D. & Zaikin, A. Superconductivity in one dimension. *Phys. Rep.* **464**, 1–70 (2008).
65. Müller, C., Cole, J. H. & Lisenfeld, J. Towards understanding two-level-systems in amorphous solids: insights from quantum circuits. *Rep. Prog. Phys.* **82**, 124501 (2019).
66. Amin, K. R. et al. Loss mechanisms in TiN high impedance superconducting microwave circuits. *Appl. Phys. Lett.* **120**, 164001 (2022).
67. Yong, J., Lemberger, T. R., Benfatto, L., Ilin, K. & Siegel, M. Robustness of the Berezinskii-Kosterlitz-Thouless transition in ultrathin NbN films near the superconductor-insulator transition. *Phys. Rev. B* **87**, 184505 (2013).
68. Bert, J. A. et al. Gate-tuned superfluid density at the superconducting $LaAlO_3/SrTiO_3$ interface. *Phys. Rev. B* **86**, 060503 (2012).
69. Mallik, S. et al. Superfluid stiffness of a $KTaO_3$-based two-dimensional electron gas. *Nat. Commun.* **13**, 4625 (2022).
70. Misra, S., Urban, L., Kim, M., Sambandamurthy, G. & Yazdani, A. Measurements of the magnetic-field-tuned conductivity of disordered two-dimensional $Mo_{43}Ge_{57}$ and InO_x superconducting films: evidence for a universal minimum superfluid response. *Phys. Rev. Lett.* **110**, 037002 (2013).

71. Turneaure, S. J., Lemberger, T. R. & Graybeal, J. M. Dynamic impedance of two-dimensional superconducting films near the superconducting transition. *Phys. Rev. B* **63**, 174505 (2001).
72. Basov, D. N. et al. In-plane anisotropy of the penetration depth in $YBa_2Cu_3O_{7-x}$ and $YBa_2Cu_4O_8$ superconductors. *Phys. Rev. Lett.* **74**, 598–601 (1995).
73. Dupré, O. et al. Tunable sub-gap radiation detection with superconducting resonators. *Supercond. Sci. Technol.* **30**, 045007 (2017).
74. Fiory, A. T., Hebard, A. F. & Glaberson, W. I. Superconducting phase transitions in indium/indium-oxide thin-film composites. *Phys. Rev. B* **28**, 5075–5087 (1983).
75. Crowley, K. D. et al. Disentangling losses in tantalum superconducting circuits. *Phys. Rev. X* **13**, 041005 (2023).
76. Wang, C. et al. Surface participation and dielectric loss in superconducting qubits. *Appl. Phys. Lett.* **107**, 162601 (2015).

Acknowledgements

We thank D. Basko, L. Benfatto, J. Delahaye, T. Grenet, V. Kravtsov, M. Müller, M. Scheffler and C. Strunk for valuable discussions. We thank É. Eyraud for assistance with the cryogenics and J. P. Martinez for the preliminary measurements. T.C. and B.S. acknowledge funding from the ANR Project No. ANR-19-CE30-0014-CP-Insulators. A.K. is grateful for support from the Laboratoire d'excellence LANEF in Grenoble (ANR-10-LABX-51-01). B.S. has received funding from the European Union's Horizon 2020 research and innovation programme under the ERC grant SUPERGRAPH no. 866365. N.R. has received funding from the European Union's Horizon 2020 research and innovation programme under the ERC grant SuperProtected no. 101001310. N.R., B.S. and D.P. acknowledge funding from the ANR agency under the 'France 2030' plan, with reference no. ANR-22-PETQ-0003. I.P. acknowledges support from the Deutsche Forschungsgemeinschaft (DFG) via grant no. MI 658/14-1.

Author contributions

T.C. designed the samples. T.C., D.P. and S.L. fabricated the samples. T.C., S.L., K.R.A., F.B. and F.G. worked on the measurement setup. T.C. and D.P. performed the measurements with initial help from S.L. T.C., B.S. and N.R. analysed the data. M.F., I.P., L.I. and A.K. developed the theory and contributed to the data analysis. B.S. and N.R. conceived the project and supervised it with O.B. B.S., T.C. and A.K. wrote the paper with inputs from all co-authors.

Competing interests

The authors declare no competing interests.

Correspondence and requests for materials should be addressed to Benjamin Sacépé.

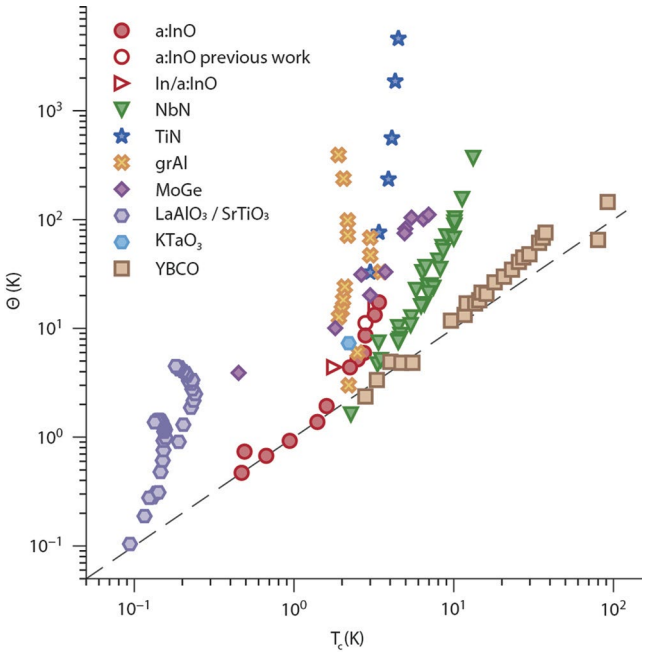

Extended Data Fig. 1 | Evolution of superfluid stiffness with critical temperature for various superconductors. Upon variation of disorder, carrier density or doping, superconductors display a decrease of both superfluid stiffness and critical temperatures. For very low superfluid densities these two quantities become of the same order, as evidenced by the dashed line representing the equality $\Theta = T_c$. a:InO lies on this line in a large disorder range. Data from[11,61,67] (NbN),[20,51] (grAl),[21,68] ($LaAlO_3/SrTiO_3$),[69] ($KTaO_3$),[15,70,71] (MoGe),[66] (TiN),[38,72] (YBCO). Previous works on a:InO[73] and In/a:InO composites[71,74] are also added.

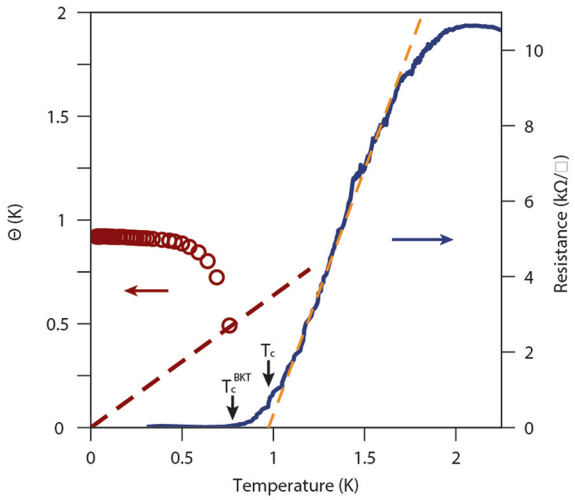

Extended Data Fig. 2 | Berezinskii-Kosterlitz-Thouless transition of sample DP-Res11. Left axis displays the superfluid stiffness versus temperature obtained from the T-dependence of the frequency shift of plasma modes via $\Theta(T) = \Theta(0)(f(T)/f(0))^2$. Dashed red line represents the Berezinskii-Kosterlitz-Thouless universal critical line $\Theta(T) = 2/\pi T$. Both curves cross exactly at the vortex unbinding temperature $T_{BKT} = 0.75$ K. Right-axis shows the corresponding superconducting transition in the sheet resistance versus temperature. The dashed orange line illustrates our definition of T_c as a linear extrapolation of the resistance curve, giving $T_c = 0.94$ K.

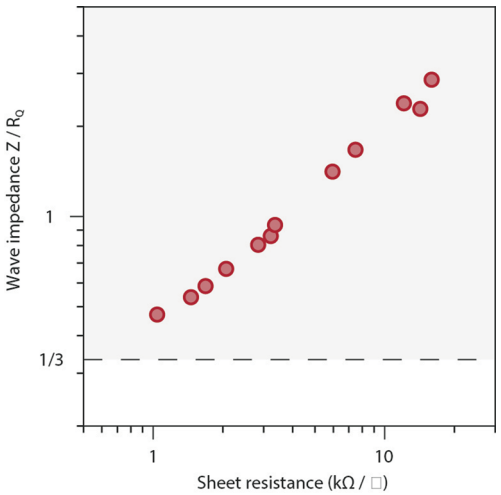

Extended Data Fig. 3 | Superinductance. Wave impedance $Z = \sqrt{l/c_1}$ versus sheet resistance. The impedance is normalized by $h/4e^2$. All data points lie well above the line $Z/(h/4e^2) = 1/3$, and some of them even achieve $Z > h/4e^2$. This classifies them as superinductances.

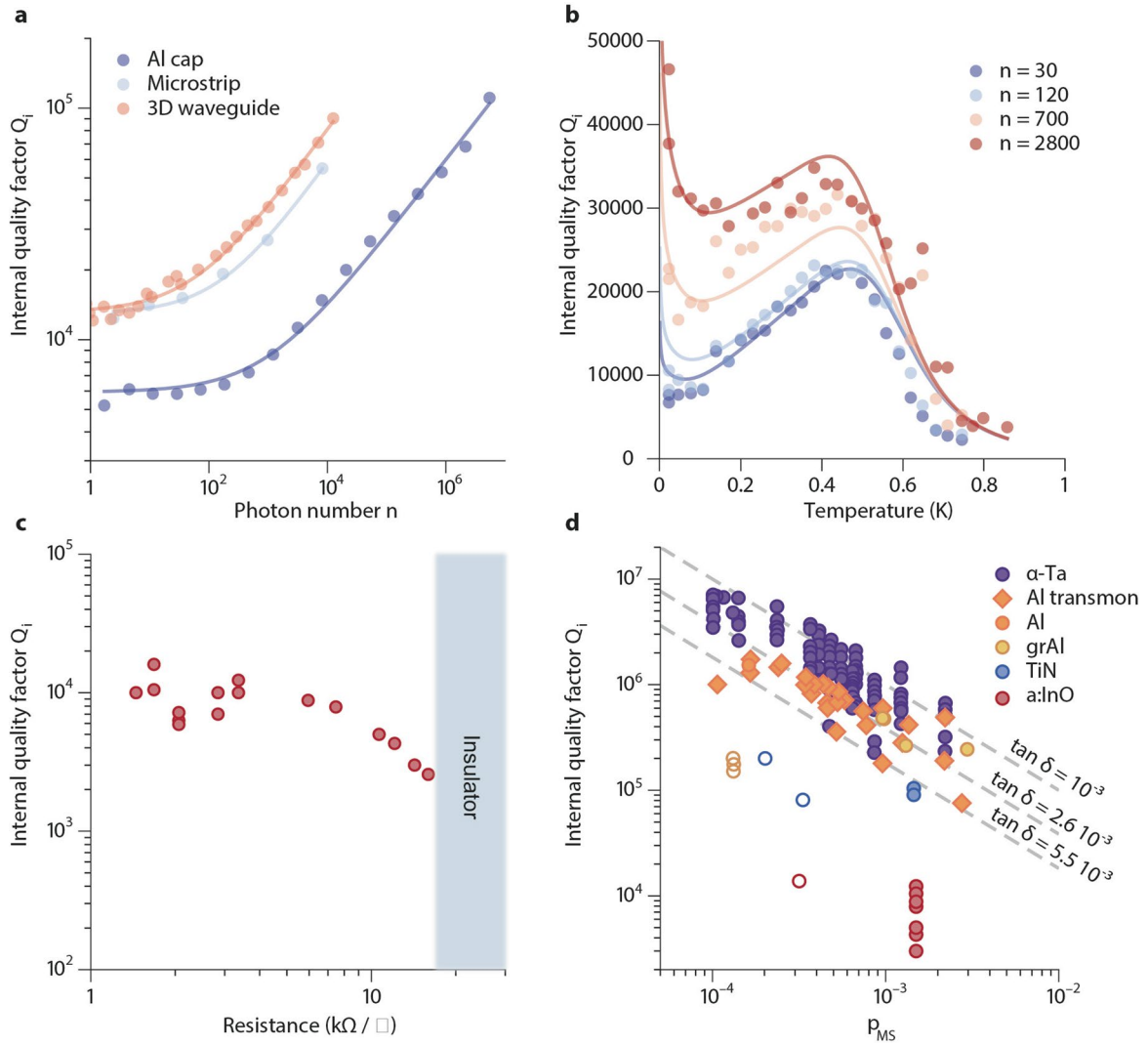

Extended Data Fig. 4 | Microwave dissipation in a:InO superconducting resonators. a Evolution of a:InO resonators quality factors upon increasing power for three different sample environments, with varying sensitivity to surface dielectric loss. We studied resonators in the microstrip geometry (see Fig. 1) or embedded in 3D aluminum waveguides (see Fig. S3) with reduced surface loss participation ratio. A third type of sample is capped in-situ after a:InO deposition by a thin aluminum layer to replace the surface dissipation of a:InO by thin aluminum oxide. **b** Temperature evolution of an a:InO resonator (sample TC040) in 3D waveguide showing non-monotonous behavior. Solid lines in panels **a** and **b** are fits following a TLS model (see SI). **c** Evolution of the low-power, low-temperature quality factor with sheet resistance, for the samples reported in Extended Table I. Near the transition to insulator the quality factor remains $>2\times10^3$. **d** Evolution of low-power and low-temperature quality factor with metal-substrate participation ratio (see SI). Full symbols correspond to resonators and transmon qubits in a 2D geometry (Ta[75], Al and grAl[59], TiN[66], Al transmons[76], a:InO), empty symbols show resonators measured in a 3D waveguide (grAl[59], TiN[66] and a:InO sample TC040). Dashed lines show the expected scaling for dielectric loss $Qi = [p_{MS} \tan\delta]^{-1}$ for three values of $\tan\delta$.

Extended Data Table 1 | Summary of experimental data discussed in the text

Sample	w (μm)	L (mm)	T_c (K)	$R_\square$ (k$\Omega/\square$)	L_K (nH/$\square$)	Θ (K)
TC002-2	1	3.505	3.4	1.04	0.452	17.35
TC002-1	1	3.505	3.2	1.456	0.59	13.29
TC014	1	2.5	3.16	1.683	0.70	11.2
TC003	1	3.5	2.8	2.06	0.91	8.6
TC040 (3D)	1	2	2.74	2.84	1.32	5.94
TC007-3	1	3.505	2.5	3.22	1.51	5.2
TC001	1	3.505	2.24	3.36	1.79	4.38
TC007-2	1	3.505	1.6	5.95	4.06	1.93
TC007-1	1	3.505	1.4	7.47	5.68	1.38
DP-res11	5	1.39	0.94	10.65	8.48	0.92
TC016-8	1	1.718	0.67	12.1	11.6	0.68
TC017	1	3.505	0.49	14.25	10.65	0.73
TC016-6	1	1.718	0.47	15.95	16.68	0.47

w and *L* are resonator width and length, respectively, T_c is the critical temperature (as discussed in Methods), and $R_\square$ is the maximum of sheet normal-state resistance measured just above T_c. L_K is obtained via fitting the plasmon dispersion relation (Methods), allowing to estimate the superfluid stiffness $\Theta = (\hbar/(2e))^2/L_K$. Note that the sample DP-Res11 (represented by squares in Fig. 1d,e) has different dimensions than the others, and thus has a dispersion relation that does not follow the disorder-evolution of the other samples, as displayed in Fig. 1d. The relation between resistance and kinetic inductance shown in Fig. 1e however is consistent with the other samples.